Warm Pool SST Variability in Relation to the Surface Energy Balance

JOHN FASULLO* AND PETER J. WEBSTER

Program in Atmospheric and Oceanic Sciences, University of Colorado, Boulder, Colorado

(Manuscript received 22 October 1997, in final form 5 June 1998)

ABSTRACT

The warm tropical oceans underlie the most convective regions on earth and are a critical component of the earth's climate, yet there are differing opinions on the processes that control warm pool SST. The Indo–Pacific warm pool is characterized by large-scale variations in SST approaching 30°C on intraseasonal timescales. In this study, surface heat flux anomalies associated with composite warm episodes over three spatial scales in both the Pacific and Indian Ocean basins are examined.

The current study benefits from the recently available National Centers for Environmental Prediction–National Center for Atmospheric Research reanalysis dataset that enables the examination of variability in surface evaporation with moderate confidence. Solar flux estimates from the reanalysis are somewhat less reliable than evaporation estimates, however, and two techniques that infer surface shortwave radiation from satellite retrievals of cloud properties are considered. Error in all measurements is quantified.

Both shortwave and evaporative flux variability play significant roles in modifying the temperature of the warm pool, though the relative importance of individual flux anomalies depends on SST tendency and geographical location. There also exist differences in the relative heating roles of the flux anomalies among episodes within a fixed location, though in instances the resolved differences are less than likely flux estimation error. Differences also exist between the ocean basins. A more pronounced annual cycle exists in the eastern Indian Ocean, and SST there is less sensitive to surface thermal forcing. Finally, the analysis offers evidence that SST is not regulated by a simple atmospheric thermodynamic response to the surface. Instead, the relationship between warm pool variability and large-scale dynamical features of the Tropics (e.g., intraseasonal oscillation and the seasonal monsoon) is demonstrated. The conclusions are shown to be robust to spatial scale and are consistent with a recent analysis of Tropical Oceans and Global Atmosphere Coupled Ocean–Atmosphere Response Experiment observations.

1. Introduction

Interactions between surface processes and atmospheric convection are among the most poorly understood aspects of the climate system and its variability. In part, progress in diagnosing these interactions has been hampered by the variety of timescales on which convection and surface fluxes fluctuate and the scarcity of datasets that sample adequately such variations.

Because of its relevance to the general circulation, the warm pool is a region where an understanding of ocean–atmosphere interactions is particularly important (e.g., Horel and Wallace 1981; Webster 1994). Figure 1 displays the climatological mean distribution of tropical sea surface temperature (SST) and outgoing longwave radiation (OLR), which serves as a proxy for deep convection. The warm pool, delineated by the 28°C isotherm, covers extensive portions of both the western Pacific and eastern Indian Oceans and about one-eight of the total area of the globe. Deep convection experiences strong spatial coherence with the warm pool. Several studies have shown tropical convection and surface winds to undergo robust variations on intraseasonal, seasonal, and interannual timescales (e.g., Madden and Julian 1994; Fu et al. 1992; Druyan and Hastenrath 1994). Associated with these variations are significant perturbations in surface heat fluxes that play an active role in modifying both the atmosphere and ocean.

There have been many theories to describe the interactions between deep convection, SST, and the surface energy balance over the warm pool. Graham and Barnett (1987) suggest that the intensity of convection over oceans warmer than 27.5°C is governed by remotely forced changes in vertical motion and stability. In contrast, Ramanathan and Collins (1991) interpret the spatial correspondence between deep convection and warm oceans as an indication that SST is regulated locally by cirrus clouds as part of a thermodynamically constrained response to the surface. Wallace (1992) suggests instead

* Current affiliation: NASA/Goddard Space Flight Center, Institute for Space Studies, Columbia University, New York, New York.

Corresponding author address: Dr. John Fasullo, NASA/GISS, Columbia University, Room 322, 2880 Broadway, New York, NY 10028. E-mail: jfasullo@giss.nasa.gov

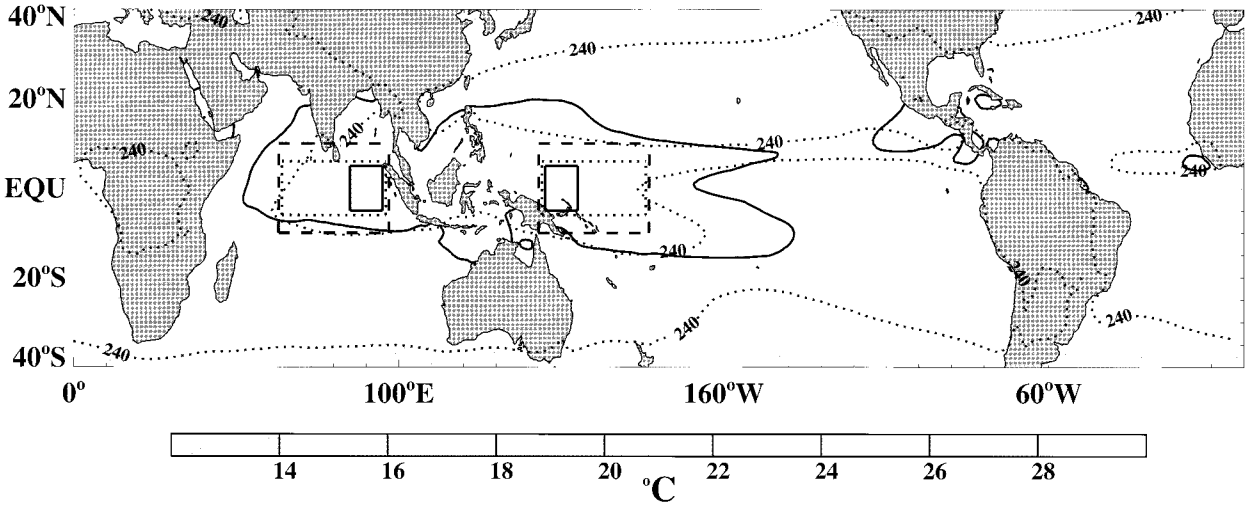

FIG. 1. The mean distribution of Reynolds SST and the 240 W m^{-2} contour (dotted) of Advanced Very High Resolution Radiometer–derived OLR. The 28°C SST isotherm is indicated (solid) and shading denotes SST at 1°C increments. Also shown are the six analysis regions (see text) outlined by solid (small scale), dotted (medium scale), and dashed (large scale) rectangular regions within the Indian and Pacific Ocean warm pool domains.

that the tropical atmosphere is especially efficient in eliminating longitudinal gradients in temperature due to the limited impact of the Coriolis force. Local SST anomalies therefore induce large-scale motions that act to cool the surface. Presumably this cooling mechanism acts through its influence on turbulent fluxes and oceanic mixing as it is strongly associated with changes in wind speed. Moreover, Hartmann and Michelsen (1993) identify evaporative anomalies as principle regulators of SST based on analysis of observations from the Tropical Ocean–Atmosphere moored buoys. Ramanathan and Collins (1992) reason, however, that as climatological mean evaporation is lower in the western Pacific than in the east, evaporation must play a secondary role in cooling the warmest oceans. Using model wind estimates and three years of satellite-derived cloud properties from International Satellite Cloud Climatology Project (ISCCP), Fu et al. (1992) show the cooling due to evaporation on interannual timescales to be much greater than that for cirrus clouds. Furthermore, in examining the phasing of convection, solar radiation, and wind fields, Fu et al. (1992) demonstrate that surface convergence precedes deep convection by 1–3 months during transitions of the seasonal cycle and therefore is not forced by SST. More recently, Lau and Sui (1997) found both evaporative and shortwave components to be important influences on Pacific warm pool SST during intraseasonal variations in convection and winds. Their conclusions are based on a several-month observational record from the improved meteorological surface mooring during the Tropical Oceans and Global Atmospheric (TOGA) Coupled Ocean–Atmosphere Response Experiment (COARE) intensive observation period (IOP; Webster and Lukas 1992).

The studies cited above exploit different analysis techniques in reaching their stated conclusions. Much of the variability sampled by Ramanathan and Collins (1991, 1992) corresponds to the presence of spatial gradients in their analysis domain. The nature of temporal fluctuations is therefore largely obscured. In contrast, the buoy data examined by Lau and Sui (1997) provides fine temporal resolution from a fixed location. The spatial and temporal brevity of their data, however, raises questions concerning its relevence to the longer and larger scale.

The goal of the current study is to investigate surface temperature and flux variability over broad domains of the Indo–Pacific warm pool using a very long-term dataset during periods in which the warm pool reaches its highest SST. The fluxes used in this analysis benefit from a more adequate treatment of the large-scale surface meteorological variations than the studies previously listed and together represent some of the most extensive estimations of daily surface flux variability currently available. Numerous warm episodes over a number of geographical domains are considered during the distinct stages of SST warming and cooling. Temporally integrated surface flux anomalies during the warm episodes will be calculated to assess their impact on oceanic heat content and SST variability. In conclusion, the role of the large-scale tropical circulation in warm pool warm episodes is discussed.

2. Data and method

a. Data

The data used in this study include

1) Reynold's SST at weekly, 1° spatial resolution (Reynolds and Smith 1994);

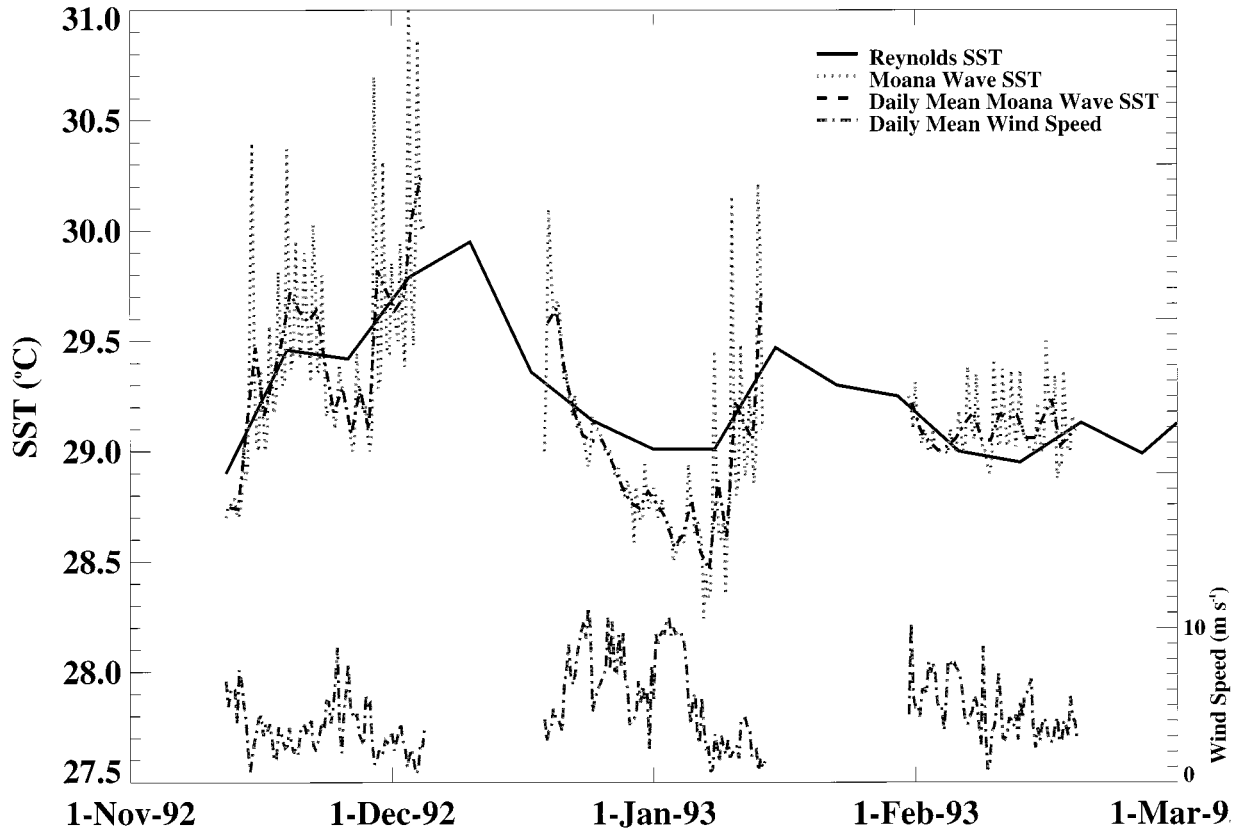

FIG. 2. (Left axis) SST and (right axis) wind speed as measured from the R/V *Moana Wave* during TOGA COARE. SST is given at both 3-h (dotted line) and daily (dashed line) resolutions. Reynolds SST is shown for comparison (solid line).

2) National Centers for Environmental Prediction (NCEP)–National Center for Atmospheric Research (NCAR) (hereafter ''the reanalysis'') reanalyzed surface evaporative and radiative fluxes at approximately 1.9°, 6-h resolution (Kalnay et al. 1996);
3) Advanced Very High Resolution Radiometer (AVHRR) OLR retrievals at 2.5° daily resolution; and
4) surface shortwave flux estimates based on International Satellite Cloud Climatology Project (ISCCP) cloud retrievals (Bishop et al. 1997).

Reynolds SST estimates are derived from an optimal interpolation technique that regresses satellite retrievals against in situ ship and buoy observations. The SST estimates are representative of temperatures at roughly 1-m depth. Figure 2 shows a comparison between Reynolds estimates and measurements of SST and wind speed from three cruises of the R/V *Moana Wave* during TOGA COARE. The first cruise is characterized by increasing SST with strong diurnal variability during a period in which winds and convection are weak (Fairall et al. 1996). The Reynolds estimates resolve adequately the weekly SST fluctuations, though they tend to understate the extent of surface warming and fail to resolve SST's diurnal cycle (Webster et al. 1996). The majority of the second and third cruises sample stronger wind conditions and are characterized by a substantially weakened SST diurnal cycle. Rms difference between the observed and Reynolds estimated SST is roughly 0.1°C on average through the three cruises.

Reanalysis evaporation estimates are based on a bulk flux parameterization that uses Reynolds SST in conjunction with the model wind, temperature, and humidity fields. Large-scale estimates of evaporation depend on several model fields, each of which contains uncertainty, and flux observations are not included in the model initialization. The suitability of the fluxes therefore needs to be established.

Figure 3 displays two comparisons of evaporation estimates, one between the reanalysis and ship measurements (Fig. 3a, from the R/V *Moana Wave* during the TOGA COARE IOP; Fairall et al. 1996), and one between the reanalysis and satellite estimates (Fig. 3b, Clayson et al. 1993). The ship–reanalysis comparison gives a strong correlation of 0.89 with a bias of 28.4 W m^{-2}. The degree of agreement is encouraging despite the wide discrepancy between the scales of comparison; the reanalysis model grid point represents an area of roughly 2.5×10^3 km^2. The rms difference between daily averaged bias-adjusted flux estimates is 48 W m^{-2},

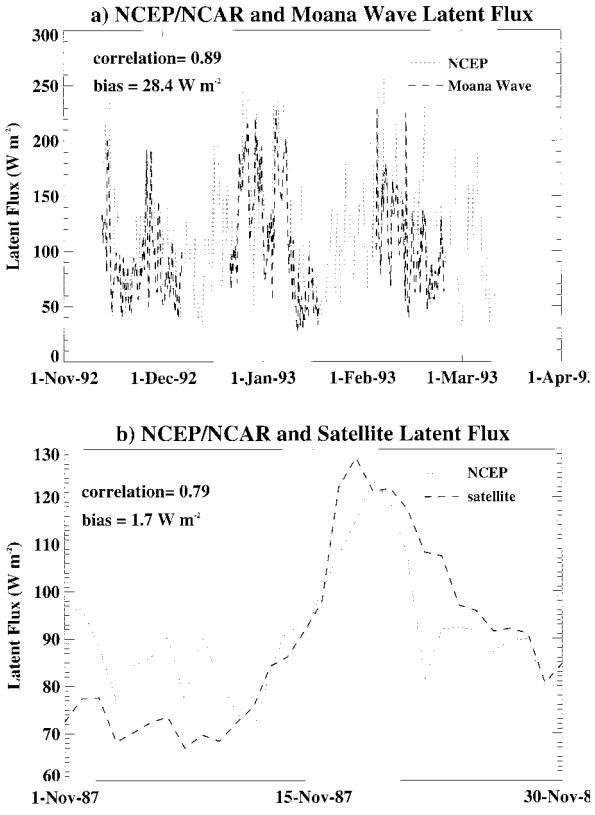

FIG. 3. Comparison of the reanalysis evaporation estimates with (a) R/V *Moana Wave* ship measurements and (b) satellite-retrieved estimates using the techniques of Clayson et al. (1993). The correlation between the time series is indicated along with the reanalysis bias.

a value that will be discussed later in error analysis. In the reanalysis–satellite comparison (Fig. 3b) made over identical portions of the western Pacific (4°S–4°N, 110°–160°E), a large correlation of 0.79 is found with a small bias of $+1.7$ W m^{-2}. The relatively strong agreement between ship observations and reanalysis and satellite estimates is not entirely unexpected as evaporative variations in the warm pool are caused predominantly by changes in surface wind speed (Liu et al. 1994), which are among the reanalysis fields most strongly influenced by observation.

Reanalysis radiative fluxes are a fully derived model product. Because the fluxes are strongly dependent on the model's cloud representation, which is sometimes poor (e.g., Hendon and Bergman 1996), two independent methods of estimating surface shortwave fluxes from satellite are used. The first method infers surface shortwave radiation from OLR (Shinoda et al. 1998) and is based on a regression against bias-adjusted surface radiation budget (SRB) experiment calculations (Whitlock et al., 1995). OLR-inferred solar radiation is useful because of the length of its available climatology. It also agrees more closely with SRB fluxes over the warm pool than do the reanalysis or empirical techniques based on cloud cover (Shinoda et al. 1998). ISCCP-retrieved solar fluxes (Bishop et al. 1997), while available over only 8 yr of our data record, result from a more explicit calculation of surface shortwave fluxes and are based on radiative modeling of ISCCP-observed cloud depth, height, and percent. Though the ISCCP method is a more direct flux calculation than the OLR technique, the shorter duration of its data record limits the number of events that can be included in warm episode composites. Consequently, estimates of surface solar flux from all of the above-mentioned sources will be examined.

A comparison between shortwave estimates based on OLR, the reanalysis, and observations from the R/V *Moana Wave* is shown in Fig. 4. The ISCCP product is unavailable during this period. OLR-inferred shortwave radiation shows the closest agreement to ship measurements with a correlation of 0.69 and a bias of $+1.7$ W m^{-2}. Rms difference between daily averaged measured and OLR inferred net solar radiation is 49 W m^{-2}. Reanalysis shortwave estimates show a modest correlation and bias (0.29, $+6.4$ W m^{-2}) and an rms difference with the shortwave observations of 64 W m^{-2}.

Components of the mean annual surface energy balance over the Pacific and Indian warm pool domains are summarized in Table 1 using different data sources. The reanalysis estimates are given along with OLR-inferred and ISCCP-calculated solar estimates.[1] For these products, both the climatological mean and temporal standard deviation are given based on daily resolved fluxes from 1982 to 1995 (1983–91 for ISCCP). Annual mean values from the climatology of Oberhuber (1988) are also given. Observational estimates from cruises by Godfrey et al. (1991) and Fairall et al. (1996) are listed, though the times of year sampled by these measurements are limited to boreal spring and winter, respectively.

The largest terms in the surface energy balance are the upwelling and downwelling longwave emissions. In the net, these terms offset each other somewhat and their variation over time is slight with standard deviations in daily averaged values near 5 W m^{-2}. The net mean longwave flux in the reanalysis is approximately 20 W m^{-2}, or about 25 W m^{-2} smaller than either the Fairall et al. (1996) or Oberhuber (1988) estimates. However, both the Fairall et al. (1996) and Oberhuber (1988) estimates are in agreement with the reanalysis in that they show variation of longwave flux over time to be slight. Sensible fluxes from the reanalysis agree with cruise estimates within 1 W m^{-2}. Like longwave fluxes, sensible flux variations over time are also small with a standard deviation of only 3–4 W m^{-2}. The most variable terms in the surface energy balance are evaporation

[1] The ISCCP product has been scaled assuming an ocean albedo of 0.06.

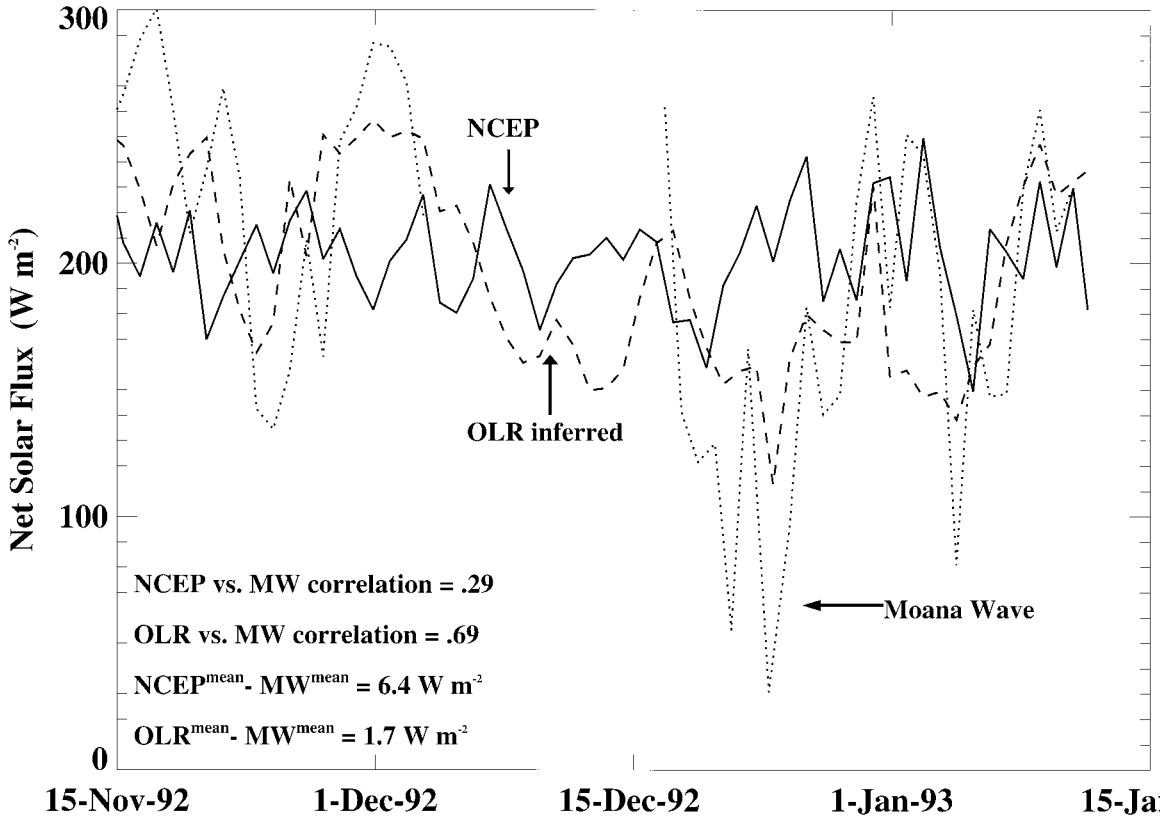

FIG. 4. Comparison between daily mean radiative fluxes as estimated by NCEP (solid), OLR inferrals (dashed), and measurements from the R/V *Moana Wave* (dotted). Correlations between time series are indicated along with the bias of each relative to ship-based measurements.

and solar radiation, which experience standard deviations of about 20–40 W m^{-2}.

Because of their variability, solar and evaporative fluxes are also the most influential modifiers of SST.

TABLE 1. Estimates of the mean surface energy balance over the Pacific and Indian Ocean warm pool. The standard deviation of daily averaged values for each flux dataset is given in parentheses.

	Evaporation	Net solar	Net longwave	Sensible
Pacific Ocean climatologies				
The reanalysis	111 (31)	197 (19)	21 (5)	8 (4)
Oberhuber	91	176	45	5
ISCCP	(n/a)	216 (37)	(n/a)	(n/a)
OLR-derived SW	(n/a)	201 (26)	(n/a)	(n/a)
TOGA COARE cruises				
Godfrey et al. (1991)	122	(n/a)	45	9
Fairall et al. (1996)	102	201	413 (up)	7.1
Indian Ocean climatologies				
The reanalysis	110 (30)	198 (18)	19 (3)	8 (3)
Oberhuber	93	171	44	5
ISCCP	(n/a)	211 (40)	(n/a)	(n/a)
OLR-derived SW	(n/a)	202 (28)	(n/a)	(n/a)

Reanalysis, OLR-inferred, and cruise-measured solar fluxes are in mutual agreement within 5 W m^{-2} over both the Indian and Pacific warm pool regions. Other flux estimates do not agree as well, however. Oberhuber (1988) and ISCCP estimates differ from other solar estimates by roughly -25 and $+15$ W m^{-2}, respectively. The difference between the ISCCP product and observations is in part due to the neglect of atmospheric aerosols in the radiative modeling as noted by Bishop et al. (1997). ISCCP-retrieved solar fluxes show the greatest temporal variability (38 W m^{-2}), followed by OLR-inferred (27 W m^{-2}) and NCEP estimates (19 W m^{-2}). The various evaporative flux estimates disagree somewhat as Oberhuber (1988) estimates are roughly 31 and 11 W m^{-2} smaller than the measurements of Godfrey et al. (1991) and Fairall et al. (1996), respectively. The reanalysis estimates are larger than those of Oberhuber (1988) and Fairall et al. (1996) but smaller than those of Godfrey et al. (1991). Thus, the mean reanalysis values do not deviate significantly from established climatologies. Temporal variability of evaporation (30 W m^{-2}) is similar in magnitude to that of solar radiation.

b. Identification of warm episodes

The variation of SST is considered in a composite analysis of extreme warm episodes over the six regions

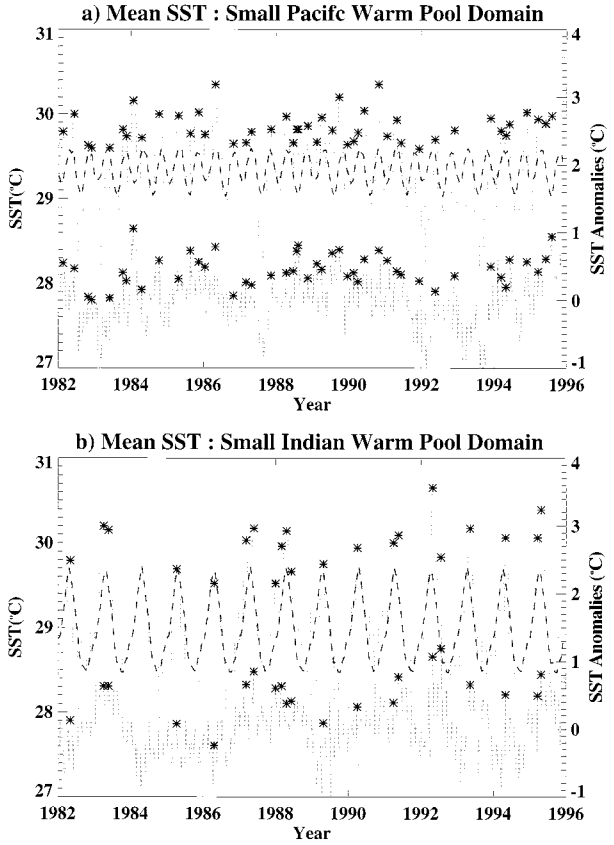

FIG. 5. Mean Reynolds SST (upper solid lines) over the small Pacific and Indian Ocean warm pool domains (Fig. 1) from 1982 through 1995. The annual cycle is shown by the dashed lines and the deviation from it is shown by the lower solid line. Warm events are marked by asterisks and are defined as the time at which SST rises above 29.5°C and is the warmest in the surrounding 9 weeks.

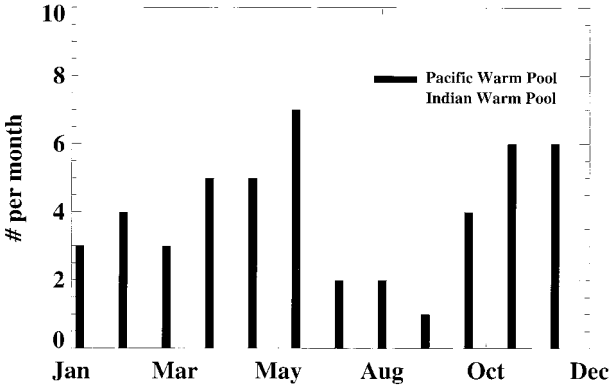

FIG. 6. The occurrence of identified warm episodes by month. A total of 48 and 21 episodes are seen over the Pacific and Indian domains, respectively.

of the Indian and Pacific domains shown in Fig. 1. Composites of warm episodes are created by identifying times at which mean SST exceeds 29.5°C and is the largest in the surrounding nine weeks. Times at which the SST meets the criteria are referred to as ''day 0.'' Notably, the criteria do not preclude the identification of any particular timescale. Flux composites are created in a linear fashion by compositing about day 0 of all episodes. Anomalies in surface energy balance terms are then calculated by removing the long-term mean (as in Lau and Sui 1997), and integrated surface heat flux anomalies are computed based on the magnitude of the flux anomalies multiplied by their duration. Heat integrations are therefore in units of J m^{-2}. Error in the fluxes and SST will be assessed under the assumption that rms deviations between the estimates and observations (section 2a) are random and are therefore governed by stochastic statistics.

The analysis of different spatial regions (described in Fig. 1) accounts for the possibility of differing SST regulation mechanisms occurring across the breadth of the Indo–Pacific warm pool and for the potentially distinct behaviors of the Indian and Pacific basins. The bulk of the analysis that follows will address composite variations in warm ocean SST over the smallest of the regions in the eastern Indian Ocean (5°N–5°S, 85°–95°E) and western Pacific Ocean (5°N–5°S, 145°–155°E) basins. Similarities and differences over the medium- and large-scale regions will then be discussed in section 3b. It should be noted than even the smallest analysis regions are extensive. The small-, medium-, and large-scale regions cover 1.2×10^6, 3.6×10^6, and 7.2×10^6 km^2, respectively. In the Indian Ocean, they are bounded by 5°S–5°N, 65°–95°E, and 10°S–10°N, 65°–95°E. In the Pacific Ocean, they are bounded by 5°S–5°N, 145°–175°E and 10°S–10°N, 145°–175°E. All regions are confined or nearly confined within the annual mean 28° SST isotherm and 240 W m^{-2} OLR isopleth in Fig. 1.

The entire time series of mean Reynolds SST over the small-scale Pacific and Indian Ocean domains from 1982 to 1995 is shown in Figs. 5a and 5b (upper solid line). Also shown are the times of identified warm episodes (asterisks), the annual cycle (dotted line), and the deviation from the annual cycle (lower solid line). Warm episodes are indicated on both the actual and deviation time series. In the Pacific, the amplitudes of the variations and the annual cycle are relatively small with a magnitude of approximately 0.5°C, and warm episodes occur roughly 80 days apart, which is similar to the timescale found by Lau and Sui (1997) for the TOGA COARE IOP. The annual cycle in the Indian Ocean has an amplitude about twice as large (1.2°C) as that in the western Pacific. Warm episodes in the Indian Ocean are also realized at the peak of intraseasonal variations, but because of the large influence of the annual cycle, there are often strong intraseasonal SST variations that do not exceed 29.5°C. This study will focus on only those events that exceed 29.5°C in order to focus attention on ocean–atmosphere interactions over the warmest oceans.

Figure 6 displays the occurrence of warm episodes

by month. In the Pacific, the episodes occur throughout the year with a modest preference for boreal spring and fall, times during which equatorial incident solar radiation at the top of the atmosphere is at its semiannual maxima. In contrast, a strong 365-day cycle is present in the Indian Ocean basin and episodes are confined to boreal springtime. The importance of this contrasting annual behavior within the ocean basins will be discussed later in the context of large-scale ocean–atmosphere interaction.

The length of the available data record allows for the compositing of multiple episodes that aid in resolving the flux variability from measurement error and undersampling. The total number of episodes identified over the Pacific and Indian small-scale domains is 48 and 21, respectively. Over the medium-scale domains, episodes total 38 and 17 over the Pacific and Indian basins, and over the large-scale domains, episodes total 18 and 14, respectively. The limited duration of ISCCP shortwave estimates reduces the number of warm episodes sampled by the data. Within the ISCCP period small-scale Pacific and Indian composites include 30 and 11 episodes, while the medium- and large-scale domains cover 23 and 10 episodes, and 14 and 6 episodes, respectively.

3. Composite intraseasonal episodes

We now calculate composite flux anomalies over small-scale domains and their integrated surface thermal forcing in the Pacific and Indian Ocean basins. A comparison is then made between the small-scale domains and the medium- and large-scale domains, followed by a discussion of variability among individual episodes and comments on the relation between the episodes and temporal variability of the Tropics, in general.

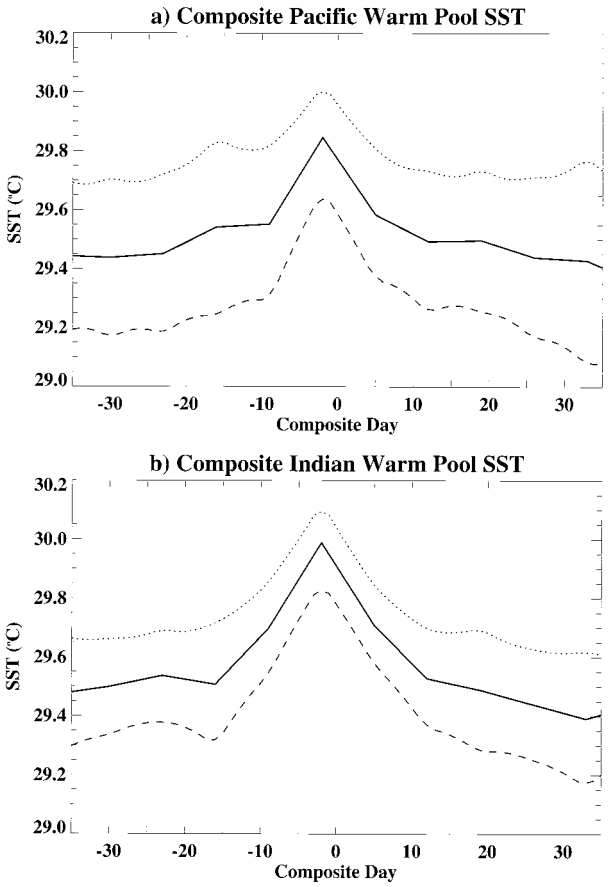

FIG. 7. Composite SST variations for the identified warm episodes (thick line) in the (a) Pacific Ocean and (b) Indian Ocean small domains. Standard deviation departures among individual events above and below the mean are indicated by the dotted and dashed lines, respectively.

a. Small-scale warm pool domains

Figure 7 shows the composite behavior of SST over both the small Indian and Pacific warm pool domains together with the standard deviation among composited events. Composite SST over the Pacific Ocean domain undergoes an increase of about 0.4°C during warm episodes, which is comparable to the magnitude of the annual cycle. Indian Ocean composite SST anomalies reach roughly 0.5°C. The composite variability of SST is much larger than a likely error in the Reynolds product, which experiences an rms deviation from TOGA COARE observations of 0.1°C and a corresponding composite error of approximately 0.02°C.

Figure 8 shows the composite behavior of reanalysis evaporation over the small domains in the western Pacific and eastern Indian Oceans. The composite SST is shown by the background dotted line and mean evaporative flux is indicated by the horizontal dashed line. During the warming phase of SST, evaporative flux in the composite is 5–15 W m^{-2} below normal during the 20 days prior to day 0. As SST cools, evaporative anomalies reach +10–+15 W m^{-2}. These anomalies are only somewhat larger than the rms uncertainty in the flux composite (6 and 10 W m^{-2} in the Pacific and Indian Ocean composites, respectively). Overall, however, the flux anomalies are consistent with the overall SST tendency and show a similar trend as the ship observations used by Lau and Sui (1997) in the TOGA COARE period.

Figure 9 shows the composite behavior of surface solar radiation as determined by the reanalysis and as inferred from OLR and ISCCP cloud properties. The mean of the reanalysis and ISCCP product composites have been adjusted for comparison (see figure caption). A number of characteristics are common to the three estimates. In the Pacific, all show elevated shortwave flux during the period in which SST warms. An abrupt transition from positive to negative shortwave anomalies occurs near day 0 as SST begins to cool. Also, positive solar anomalies return at approximately day 24, an occurrence similar to that observed by Lau and Sui (1997), who attributed subsidence in their analysis re-

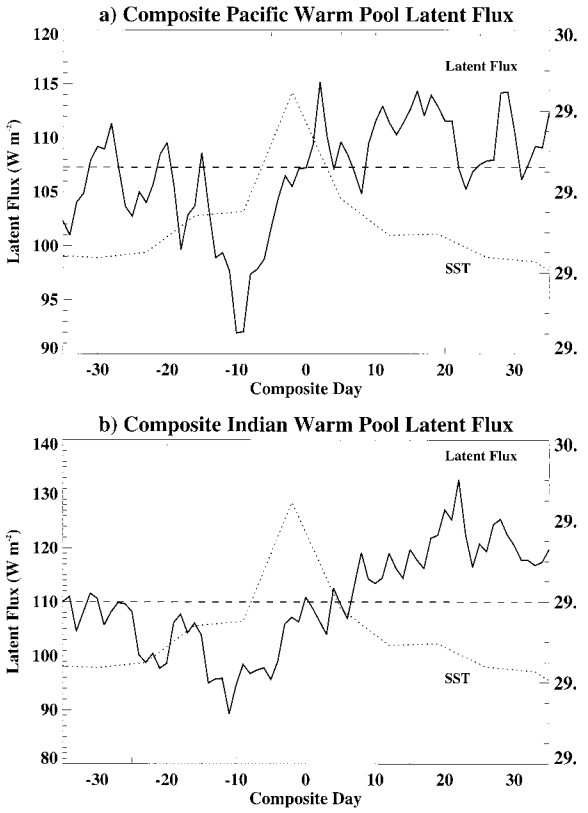

FIG. 8. Composite evaporative flux over the small (a) Pacific and (b) Indian Ocean warm pool domains. Climatological mean evaporation at day 0 is also given (dashed). Evolving composite SST (right axis) is shown for reference (dotted).

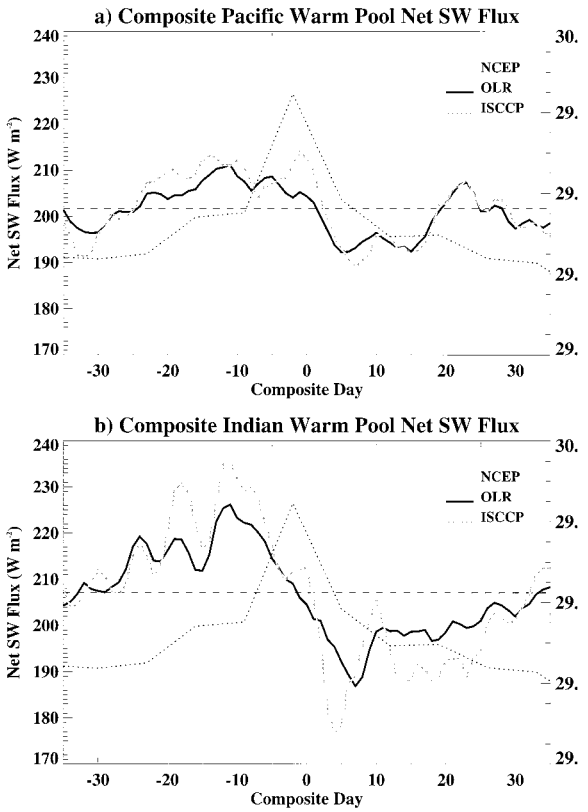

FIG. 9. Composite net shortwave flux over the (a) Pacific and (b) Indian Ocean small domains as depicted by both OLR inferrals (black), NCEP estimates (dashed gray), and ISCCP estimates (solid gray). Bias in the mean of the various estimates is adjusted to coincide with the mean OLR estimate. The adjustment for reanalysis estimates is 4 W m^{-2} and for ISCCP estimates is 3.5 W m^{-2}. Composite mean net shortwave fluxes at day 0 are given by the horizontal dashed line. Evolving composite SST is also shown for reference (dotted).

gion to the dynamic influence of remote convection. This possibility will be explored further in section 4.

In the Indian Ocean warm pool, a marked transition from positive to negative solar anomalies near day 0 is again apparent in all estimates. Peak to trough variability is considerably larger in the Indian Ocean domain than in the Pacific, and the ISCCP product shows the greatest variability of the available estimates. Unlike the Pacific domain, no return to above normal surface heating is realized within 35 days after day 0 by any of the estimates, raising the possibility that different large-scale processes govern the Indian Ocean domain. This possibility will also be examined in section 4.

The time-integrated impact of flux anomalies on the surface energy balance is now investigated to quantify the relative roles of individual fluxes in surface thermal forcing. Heating anomalies are calculated from the difference between daily mean fluxes and the long-term mean for each flux (Figs. 9, 10). Rms daily flux error is estimated from the difference between the estimates and observations (section 2) and error is assumed stochastic. Error in the heat integrations therefore varies as $1/n^{0.5}$, where n is the number of events in the composite multiplied by the number of days integrated. Uncertainty in the 35-day integrated energy associated with reanalysis latent flux and OLR inferred solar flux anomalies are approximately 9.0×10^5 and 1.4×10^6 J m^{-2} in the Pacific and Indian Ocean composites, respectively. Integrated energy anomalies associated with reanalysis shortwave flux are 1.2×10^6 and 1.8×10^6 J m^{-2} in the Pacific and Indian Ocean composites, respectively. The maximum likely error in the ISCCP shortwave calculation estimated by Bishop et al. (1997) is 50 W m^{-2} and, as a reduced number of samples is included in the composite, rms error in the ISCCP product heat integrations is somewhat greater than for the other flux estimates at 1.1×10^6 and 2.0×10^6 J m^{-2} for the Pacific and Indian Ocean basins, respectively.

Table 2 summarizes the integrated heating anomalies of the small warm pool domains by flux term and SST tendency. Figure 10 displays the time evolution of anomalous heat accumulation due to each flux. In the Pacific Ocean composite, the estimates show important and nearly equal roles for evaporative and shortwave anomalies in both the warming and cooling of SST. Total

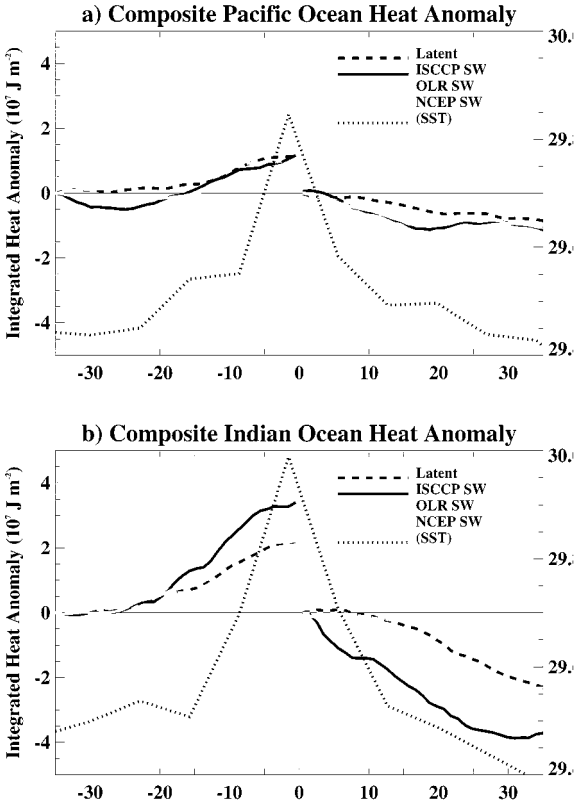

FIG. 10. Temporally integrated heat flux anomalies due to evaporation (dark dashed), ISCCP inferred solar radiation (dark solid), OLR inferred shortwave radiation (solid gray), and reanalysis solar radiation (dashed gray). Integrations are carried out from day −35 to day −1 and from day 1 to day 35, representative of the warming and cooling phases of SST respectively. SST is also plotted for reference (dotted).

thermal forcing due to evaporative and solar fluxes is approximately an order of magnitude greater than for sensible and longwave fluxes.

Evaporative and solar flux anomalies also dominate the perturbation to the surface energy balance in the Indian Ocean. The Indian Ocean heat flux anomalies in the 35 days around day 0 are roughly twice as large as those in the Pacific, though the overall SST tendency is only about 20% greater. The discrepancy suggests that Indian Ocean mixed layer characteristics such as its depth and transfer of heat may differ from those in the Pacific as found by Loschnigg and Webster (1997). Nevertheless, the overall SST tendency is consistent with the sign of the estimated surface thermal forcing in both basins. In the Indian Ocean, considerable disagreement exists among surface solar flux estimates, with ISCCP showing nearly three times as much surface thermal forcing as the reanalysis estimates. On average, evaporation and solar flux perturbations share nearly equal roles in total surface thermal forcing.

TABLE 2. Total integrated flux anomalies during the 35-day warming and cooling phases of SST for both the Pacific and Indian Ocean domains. All estimates are from the reanalysis except for shortwave estimates from OLR and ISCCP as indicated. Units are 10^6 J m^{-2}. Magnitude of the composite SST warming and cooling phases are also given next to the ocean basin designation.

	Small-scale ocean domains			
	Pacific Ocean (0.49°C)		Indian Ocean (0.69°C)	
Flux term	Warming	Cooling	Warming	Cooling
Evap.	11.8	−8.5	21.9	−23.1
SW (OLR)	7.8	−10.3	21.3	−23.6
SW (ISCCP)	13.0	−10.0	33.8	−37.1
SW (NCEP)	10.7	−10.2	12.5	−14.2
Longwave	−2.2	1.3	−1.2	2.3
Sensible	0.8	−0.9	−0.5	0.6

TABLE 3. As in Table 2 except for medium-scale domain.

	Medium-scale ocean domains			
	Pacific Ocean (0.40°C)		Indian Ocean (0.89°C)	
Flux term	Warming	Cooling	Warming	Cooling
Evap.	4.5	−6.6	28.4	37.9
SW (OLR)	11.4	−9.5	20.0	−21.7
SW (ISCCP)	19.6	−9.5	35.5	−33.7
SW (NCEP)	6.4	−6.6	20.8	−22.0
Longwave	−2.0	1.3	−3.0	3.5
Sensible	0.1	−0.6	0.6	−1.5

b. *Spatial-scale dependence*

Tables 3 and 4 summarize the integrated heat flux anomalies for the medium- and large-scale domains, respectively. The magnitude of SST variations is similar across all domains in the Pacific warm pool but increases with domain size in the Indian Ocean. Evaporative and shortwave flux anomalies dominate perturbations to the surface energy balance in both basins and over all scales, as longwave and sensible integrated flux anomalies remain below 3×10^6 J m^{-2} in the Pacific domains and 7×10^6 J m^{-2} in the Indian Ocean domains. There exist some distinctions between the domains, however. Over the medium-scale Pacific domains, the role of latent heat flux anomalies in the warming phase of SST is somewhat reduced from the small-scale domain, while in the

TABLE 4. As in Table 2 except for large-scale domains.

	Large-scale ocean domains			
	Pacific Ocean (0.47°C)		Indian Ocean (0.98°C)	
Flux term	Warming	Cooling	Warming	Cooling
Evap.	9.3	−9.8	41.8	−46.8
SW (OLR)	12.2	−5.4	22.1	−27.8
SW (ISCCP)	19.8	−9.0	41.1	−46.7
SW (NCEP)	12.7	−11.4	27.4	−33.4
Longwave	−2.8	1.2	−5.1	6.8
Sensible	0.2	−0.5	0.7	−1.5

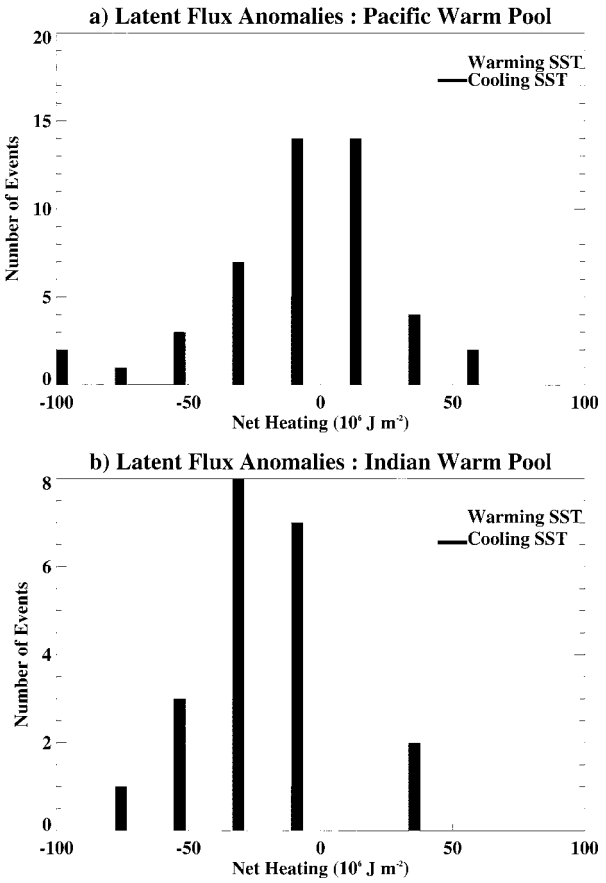

FIG. 11. The distribution of integrated heat flux anomalies associated with evaporative anomalies during the warming (light) and cooling (dark) phases of SST for individual episodes over the (a) Pacific and (b) Indian Ocean domains.

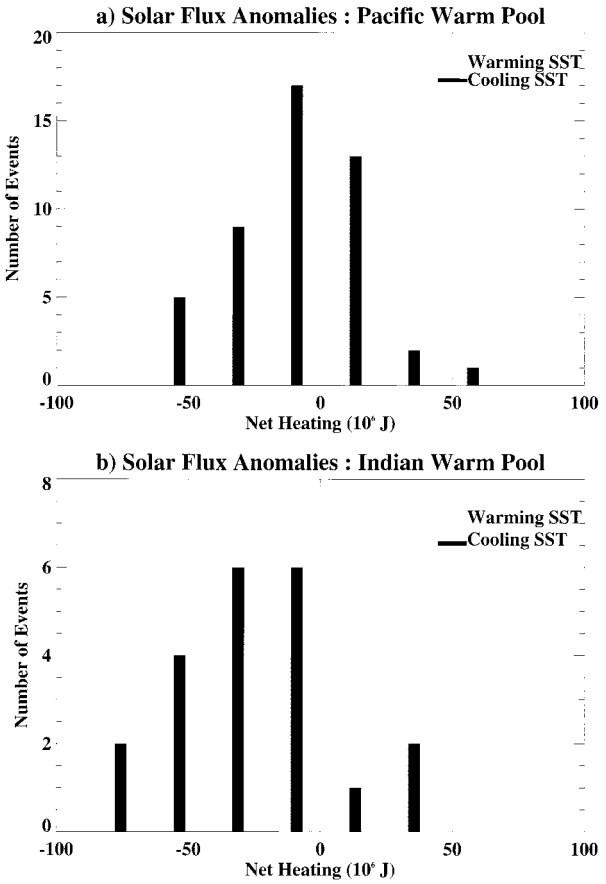

FIG. 12. As in Fig. 11 except for OLR-inferred solar flux anomalies.

medium- and large-scale Pacific domains, ISCCP estimates show an increasingly important role for solar anomalies in the warming phase of SST. An increased role for solar anomalies in cooling the surface over the medium- and large-scale Pacific domains is not apparent, however. In the Indian Ocean, the role of evaporation in both the warming and cooling phases of SST increases with domain size while the magnitude of solar flux variability is approximately independent of scale. Over a wide variety of scales, therefore, evaporation and solar radiation exert an important influence on warm pool SST.

c. Variability between warm episodes

In diagnosing the feedback between the ocean and atmosphere, Lau and Sui (1997) studied a single warm episode during the TOGA COARE IOP. It has been demonstrated that this episode displays many characteristics of the composite warm episodes studied here. However, it is unclear to what extent variability in surface flux anomalies exists between individual episodes in the composite analysis. To complement the composites, therefore, the variability among episodes is examined.

Figure 11 displays the distribution of integrated latent flux anomalies for all warm episodes. Unlike the composite heat integrations, these calculations are based on single occurrences and are therefore susceptible to a greater degree of uncertainty. Latent flux error is estimated at approximately 6×10^6 J m^{-2} given the 35 daily samples in each integration and the rms daily flux error of section 2. Notwithstanding likely error, strong variability in flux anomalies is apparent and at times evaporative anomalies act counter to the observed SST tendency. Warming and cooling distributions are more distinct in the Indian Ocean domains than in the Pacific, a characteristic that may reflect the different associations between episodes and the annual cycle (Fig. 6). In the Pacific basin, episodes are driven predominantly by intraseasonal atmospheric variations, whereas in the Indian basin episodes are also strongly influenced by a strong and sustained seasonal cycle. The relevance of these variations to maintenance of the warm pool will be discussed further in section 3d.

Figure 12 shows the distribution of integrated solar

flux anomalies among episodes. As for latent fluxes, error in these integrations is estimated at 6×10^6 J m^{-2}. Significant variability between episodes exists and solar anomalies act counter to the overall SST tendency in instances. As with evaporative anomalies, solar fluxes in the Indian Ocean act more consistently in agreement with the overall SST tendency than in the Pacific, as evidenced by a more clear distinction between warming and cooling distributions in the Indian Ocean.

d. Timescale dependence

The Tropics are unique because maximum solar irradiance is incident at the top of the atmosphere two times per year and semiannual variability can therefore exceed annual variability in places. Dynamical systems in the proximity of the warm pool, such as the Asian monsoon, also introduce a very pronounced annual harmonic by modifying the circulations of the ocean and atmosphere and the distribution of clouds. The initial identification of warm episodes (Fig. 6) suggests that the two harmonics exert disproportionate influences over the warm pool basins. The Pacific domain SST exhibits a noticeable semiannual cycle with frequent spring and fall warm episodes while the Indian Ocean basin is dominated by a strong annual cycle, which limits the occurrence of episodes to boreal spring. Thus, the local top-of-the-atmosphere solar flux does not alone control the seasonal changes of SST. Instead, the large-scale circulation, through its association with clouds and wind-induced currents, mixing, and evaporation, exerts a strong influence as well.

Boreal spring represents a period of marked transition for the Indian Ocean basin because it is accompanied by the onset of the south Asian monsoon. The monsoon drives sustained winds, which in turn drive vigorous currents in the Indian Ocean (Knox 1987). These currents and their associated transports of heat and momentum are responsible for the large annual cycle in SST in the Indian Ocean (Loschnigg and Webster 1997). Near the time of the initial monsoon onset, warm episodes are often observed, yet as the monsoon becomes established, SST near the equator cools. Therefore, although intraseasonal variations in surface heat flux associated with the established Asian monsoon are strong and important, they experience only limited association with changes in near-equatorial SSTs bounding 29.5°C.

In contrast, oceanic heat flux divergence in the western Pacific warm pool is small and is often set to zero in numerical simulations of the ocean–atmosphere system (e.g., Seager et al., 1995). The annual and semiannual variations in SST are therefore largely forced by surface heat flux variations. Changes in composite fluxes during warm episodes are more rapid than in the Indian Ocean basin and spectral analysis of OLR-inferred solar anomalies display a pronounced spectral peak near 50 days, a peak that has previously been observed in both clouds and winds (see Madden and Julian 1994 for a review). In the western Pacific, it is therefore suggested that deep convection and low-level winds associated with intraseasonal disturbances such as westerly wind bursts account for a large degree of the atmosphere's cooling influence (Fasullo and Webster 1999). The above possibilities suggest that an examination of the large-scale circulation is appropriate.

4. Large-scale associations

Figure 13 shows the large-scale evolution of anomalous OLR about day 0 during three time periods associated with warm episodes in the small-scale warm pool regions. The periods correspond to the warming (days -15 to -5), peak (days -5 to 5), and cooling (days 5 to 15) phases of warm pool warm episodes. The features of these distributions are nearly identical to those resolved in composites for the medium- and large-scale warm episodes (not shown). It is remarked that the signal in OLR in Fig. 13 is substantially greater that the noise induced by temporal undersampling of convection, which is roughly 1.0 W m^{-2} for the Pacific composite and twice that for the Indian composite.[2]

During the composite warming phase of Pacific SST (Fig. 13a), deeper than normal convection exists over the Indian Ocean while convectively inactive conditions exist in the western Pacific. Convection evolves in a manner similar to that associated with the intraseasonal oscillation, moving eastward at approximately 5 m s^{-1}. At the peak of SST (Fig. 13b), deep convective and subsident conditions bound the study area. Cooling of the Pacific warm pool (Fig. 13c) coincides with local deep convection over Indonesia, the far western Pacific Ocean, and the South China Sea, while weak convection prevails over the Indian Ocean. The association of warm episodes in the Pacific with the intraseasonal oscillation as interpreted by Lau and Sui (1997) is therefore consistent with the extended data record.

The reorganization of convection associated with composite SST fluctuations in the Indian Ocean is somewhat different from that seen in the Pacific and is shown in Figs. 13d–13f. During the warming phase of SST (Fig. 13d), convection is strong over eastern Africa and southwest Asia and weak over most of the equatorial Indian and western Pacific Oceans. As SST in the study area peaks (Fig. 13e), the study area is straddled by deep convection to its west and reduced convection to its east, with large-scale OLR anomalies greater than 10 W m^{-2}. A complex redistribution of convection over

[2] Maximum likely error in OLR induced by temporal undersampling of convection is approximately 30 W m^{-2}. The error is stochastic and therefore decreases as $1/n^{0.5}$. In the Pacific composite 10 days from each of the 48 episodes are included. In the Indian composite 10 days from each of the 21 episodes are included, resulting in a sampling error of 1.4 and 2.1 W m^{-2} for the Pacific and Indian Ocean basins, respectively.

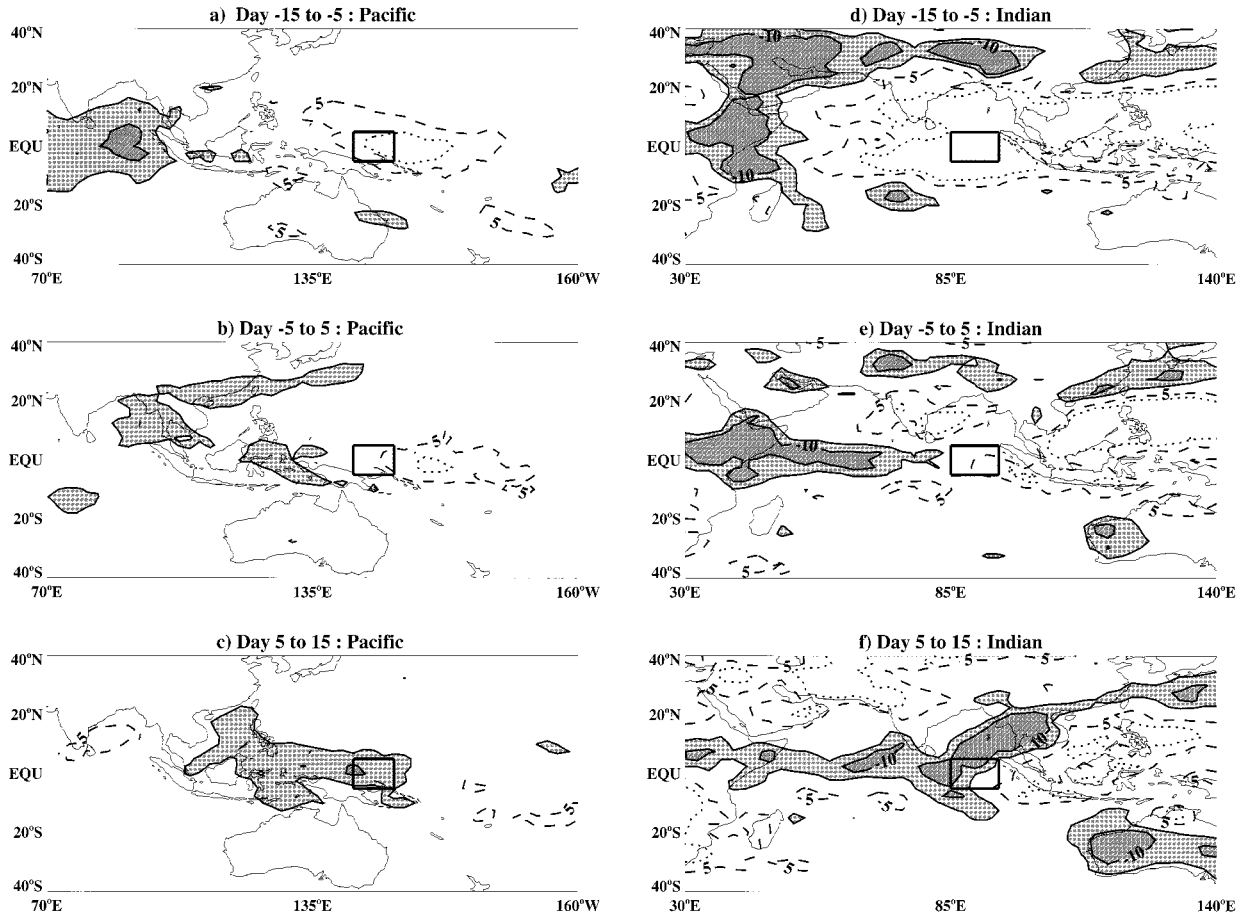

FIG. 13. Composite OLR anomalies associated with the warming, peak, and cooling phase of SST in the Pacific [(a), (b), (c)] and Indian [(d), (e), (f)] domains. Deeper than normal convection (dark shading, solid contours) corresponds to anomalies of -5 to -10 W m^{-2} and shallow convection (light, dashed contours) corresponds to anomalies of $+5$ to $+10$ W m^{-2}.

southern Asia is also apparent and is associated with the monsoon onset as discussed by Webster et al. (1998). SST cooling (Fig. 13f) is accompanied by strong convection over the entire equatorial Indian Ocean, southeastern Asia, and Australia. Convectively inactive conditions cover southwest Asia, off-equatorial Africa, and the western Pacific Ocean. As early June corresponds to the mean onset date of the Asian monsoon (Rao 1976), warm episodes in the Indian Ocean tend to precede the monsoon wet season by a few weeks. Precursors of the monsoon onset, such as the presence of strong equatorial convection (Yasanuri 1979) and consequent oceanic currents forced by the established monsoon, are apparently responsible for cooling the equatorial warm pool below its warmest SSTs. The branched pattern seen in Fig. 13f, where convection extends along the equator in the western Indian Ocean and into the subtropics east of 90°E, is similar to fundamental modes of intraseasonal variability in convection shown by Wang and Rui (1991) and active-break transitions of the Asian monsoon (Webster et al. 1998). Furthermore, Nicholls (1989) notes that 40% of the rainfall variability during winter over Australia can be explained by this pattern and is related to an SST dipole between Indonesia and the eastern Indian Ocean. Wang and Rui (1991) also demonstrate that similar convective variations are important characteristics of tropical intraseasonal variability throughout the year, and it is therefore incorrect to view the pattern as a unique atmospheric signature of SST in excess of 29.5°C.

The presence of coherent large-scale atmospheric anomalies is relevant to the examination of previous studies. A premise of Ramanathan and Collins (1991, 1992) is that nature of temporal variability can be inferred from spatial variations. That is, spatial gradients in SST, surface fluxes, and convection across the Pacific Ocean display similar associations to temporal variability over a fixed location. There is little evidence to support the supposition that spatial variations in clouds and SST are indicative of temporal feedbacks, however. It is known that gradients in SST and convection across the Pacific are important characteristics of the Walker circulation, a dynamical feature influenced by lateral heating gradients across the Pacific and Indian Oceans.

Ascent over the warm pool is therefore not only influenced by local heating, but by the strength of such gradients, which can potentially change independently of fluctuations in warm pool SST. A unique correspondence between the surface and local cloud radiative forcing and evaporation therefore cannot exist. Aside from daily excursions associated with the diurnal cycle, the warm pool attains its warmest SST on intraseasonal timescales and is strongly influenced by variations in wind and convection, which propagate in space. The warm pool cannot therefore be viewed as a closed system. That is, attempts to characterize the tendency of convection based solely on the underlying SST are incorrect and analysis attempts to characterize changes in surface temperature via exact differentials in surface fluxes are therefore poorly posed.

5. Conclusions

The SST of the western Pacific Ocean warm pool experiences some semiannual tendency but warm episodes (>29.5°C) can occur throughout the year. The Indian Ocean is characterized by a greater annual cycle than in the western Pacific Ocean and temperatures greater than 29.5°C are only realized during boreal spring. Variations in surface fluxes suggest an important role for intraseasonal variations in clouds and wind in modifying SST, and evaporative and solar fluxes are together the dominant modifiers of the surface energy balance. Also, the warm episode studied by Lau and Sui (1997) appears largely representative of warm episodes in general as assessed over a variety of spatial scales.

Finally, the strong correlation between SST variations and large-scale convective anomalies suggest that SST cannot be understood in terms of local interactions between thermodynamics, convection, and radiation. Instead, outbreaks of convection are associated with changes in dynamical systems such as the intraseasonal oscillation and the Asian monsoon. Those studies that suggest a local correspondence between SST and evaporation or shortwave cloud forcing are therefore incomplete. An understanding of the interaction between large-scale dynamic systems and the surface is prerequisite to understanding the maintenance of the warm pool.

Acknowledgments. This work was funded by NSF Grant ATM-9525847 and DOE Grant DE-FG03-94ER61770. The authors would also like to thank J. Curry and W. B. Rossow for their assistance during revisions. NCEP–NCAR reanalysis data were provided through the NOAA Climate Diagnostics Center (http://www.cdc.noaa.gov).

REFERENCES

Bishop, J. K. B., W. B. Rossow, and E. G. Dutton, 1997: Surface solar irradiance from the International Satellite Cloud Climatology Project 1983–1991. *J. Geophys. Res.,* **102,** 6883–6910.

Clayson, C. A., J. A. Curry, W. B. Rossow, and P. J. Webster, 1993: Determination of the tropical sea surface energy balance from satellite. Preprints, *20th Conf. on Hurricanes and Tropical Meteorology,* San Antonio, TX, Amer. Meteor. Soc., 591–594.

Druyan, L. M., and S. Hastenrath, 1994: Tropical impacts of SST forcing: A case study for 1987 versus 1988. *J. Climate,* **7,** 1316–1323.

Fairall, C. W., E. F. Bradley, D. P. Rogers, J. B. Edson, and G. S. Young, 1996: Bulk parameterization of air–sea fluxes for TOGA COARE. *J. Geophys. Res.,* **101** (C2), 3747–3764.

Fasullo, J., and P. J. Webster, 1999: Ocean–atmosphere interaction during strong westerly wind bursts. *Quart. J. Roy. Meteor. Soc.,* in press.

Fu, R., A. D. Del Genio, W. B. Rossow, and W. T. Liu, 1992: Cirrus-cloud thermostat for tropical sea surface temperatures tested using satellite data. *Nature,* **358,** 394–397.

Godfrey, J. S., M. Nunez, E. F. Bradley, P. A. Coppin, and E. J. Lindstrom, 1991: On the net surface heat flux into the western equatorial Pacific. *J. Geophys. Res.,* **96,** 3391–4000.

Graham, N. E., and T. P. Barnett, 1987: Sea surface temperature, surface wind divergence, and convection over tropical oceans. *Science,* **238,** 657–659.

Hartmann, D. L., and M. L. Michelsen, 1993: Large-scale effects on the regulation of tropical sea surface temperature. *J. Climate,* **6,** 2049–2062.

Hendon, H., and J. Bergman, 1996: The impact of cloud distributions in the seasonal cycle of radiative heating at the surface and in the atmosphere. *Proc. 21st Annual Climate Diagnostics and Prediction Workshop,* Huntsville, AL, U.S. Dept. of Commerce, 356–369.

Horel, J. D., and J. M. Wallace, 1981: Planetary-scale atmospheric phenomena associated with the Southern Oscillation. *Mon. Wea. Rev.,* **109,** 813–829.

Kalnay, E., and Coauthors, 1996: The NCEP/NCAR 40-Year Reanalysis Project. *Bull. Amer. Meteor. Soc.,* **77,** 437–471.

Knox, R., 1987: The Indian Ocean: Interaction with the monsoon. *Monsoons,* J. S. Fein and P. Stevens, Eds., John Wiley and Sons, 2365–2398.

Lau, K.-M., and C.-H. Sui, 1997: Mechanisms of short-term sea surface temperature regulation: Observations during TOGA COARE. *J. Climate,* **10,** 465–472.

Liu, W. T., A. Zhang, and J. Bishop, 1994: Evaporation and solar irradiance as regulators of sea surface temperature in annual and interannual changes. *J. Geophys. Res.,* **99,** 9959–9974.

Loschnigg, J., and P. J. Webster, 1996: SST regulation in the Indian Ocean: A counterpoint to the Pacific warm pool. Preprints, *Conf. on Global Ocean–Atmosphere–Land Systems (GOALS),* Atlanta, GA, Amer. Meteor. Soc., 136–139.

Madden, R. A., and P. R. Julian, 1994: Observations of the 40–50 day tropical oscillation—A review. *Mon. Wea. Rev.,* **122,** 815–837.

Nicholls, N., 1989: Sea surface temperatures and Australia winter rainfall. *J. Climate,* **2,** 965–973.

Oberhuber, J. M., 1988: An atlas based on the 'COADS' data set: The budgets of heat, buoyancy and turbulent kinetic energy at the surface of global ocean. Max-Planck Institut für Meteorologie Rep. 15, 20 pp. [Available from the Max-Plank Institut für Meteorologie, Bundsstrasse 55, 20146 Hamburg, Germany.]

Ramanathan, V., and W. Collins, 1991: Thermodynamic regulation of ocean warming by cirrus clouds deduced from observations of the 1987 El Niño. *Nature,* **351,** 27–32.

——, and ——, 1992: Thermostat and global warming, *Nature,* **357,** 649.

Rao, Y. P., 1976: Southwest monsoon. *Synoptic Meteorology, Meteor. Monogr.,* No. 1, India Meteorological Department, 367 pp.

Reynolds, R. W., and T. M. Smith, 1994: Improved global sea surface temperature analyses using optimum interpolation. *J. Climate,* **7,** 929–948.

Seager, R., M. B. Blumenthal, and Y. Kushnir, 1995: An advective atmospheric mixed layer model for ocean modeling purposes:

Global simulation of surface heat fluxes. *J. Climate,* **8,** 1951–1964.

Shinoda, T., H. H. Hendon, and J. Glick, 1998: Intraseasonal variability of surface fluxes and sea surface temperature in the tropical western Pacific and Indian Oceans. *J. Climate,* **11,** 1685–1702.

Wallace, J. M., 1992: Effect of deep convection on the regulation of tropical sea surface temperature. *Nature,* **357,** 230–231.

Wang, B., and H. Rui, 1991: Synoptic climatology of transient tropical intraseasonal convection anomalies: 1975–1985. *Meteor. Atmos. Phys.,* **44,** 43–61.

Webster, P. J., 1994: The role of hydrological processes in ocean–atmosphere interaction. *Rev. Geophys.,* **32,** 427–476.

——, and R. Lukas, 1992: TOGA COARE: The Coupled Ocean–Atmosphere Response Experiment. *Bull. Amer. Meteor. Soc.,* **73,** 1377–1416.

——, C. A. Clayson, and J. A. Curry, 1996: Clouds, radiation, and the diurnal cycle of sea surface temperature in the tropical western Pacific Ocean. *J. Climate,* **9,** 1712–1730.

——, V. Magana, T. N. Palmer, J. Shukla, M. Yanai, and T. Yasunari, 1998: Monsoons: Processes, predictability and the prospects for prediction. *J. Geophys. Res.,* **103,** 14 395–14 451.

Whitlock, C.H., and Coauthors, 1995: First global WCRP shortwave surface radiation budget dataset. *Bull. Amer. Meteor. Soc.,* **76,** 905–922.

Yasunari, T., 1979: Cloudiness fluctuations associated with the Northern Hemisphere summer monsoon. *J. Meteor. Soc. Japan,* **57,** 227–242.